Cavitation Mean Expectation Time in a Stretched Lennard-Jones Fluid under Confinement

Mathieu Pellegrin, Yann Bouret, Franck Celestini, Xavier Noblin

Cavitation mean expectation time in a stretched Lennard-Jones fluid under confinement

Mathieu Pellegrin, Yann Bouret, Franck Celestini, and Xavier Noblin*

Université Côte d'Azur, CNRS, Institut de Physique de Nice UMR7010 (INPHYNI), Parc Valrose 06108 Nice Cedex 2, France

E-mail: xavier.noblin@unice.fr

Abstract

We investigate the nucleation of cavitation bubbles in a confined Lennard-Jones fluid submitted to negative pressures in a cubic enclosure. We perform molecular dynamics (MD) simulations with tunable interatomic potentials that enable to control the wettability of the solid walls by the liquid, i.e its contact angle. For a given temperature and pressure, as the solid is taken more hydrophobic, we put in evidence an increase of the nucleation probability. A Voronoi tessellation method is used to accurately detect the bubble appearance and its nucleation rate as a function of the contact angle. We adapt the Classical Nucleation Theory (CNT) proposed for the heterogeneous case on a flat surface to our situation where bubbles may appear flat walls, edges or corner of the confined box. We finally calculate a theoretical mean expectation time in these three cases. The ratio of these calculated values over the homogeneous case is computed and compared successfully against MD simulations. Beyond the infinite liquid case, this work explore the heterogeneous nucleation of cavitation bubble, not only in the flat surface case, but for more complex confining geometries.

INTRODUCTION

Bubble nucleation from a mestastable liquid is a common phenomenon that can be observed by increasing its temperature above the boiling point, or by decreasing the liquid pressure below the vapor pressure.[1] The first case has strong technological relevance for heat exchangers[2] and can lead to severe accidents in the chemical industry by explosive boiling.[3] We focus here on the second case, where the pressure decrease can be transient or quasi-static, leading to the nucleation of a bubble by over-passing an energy barrier. The transient case presents several applications, ranging from acoustic cavitation for medicine[4] or sonochemistry[5] and hydraulic cavitation past boat helices.[6] For a long time it has also been known that stretched liquid in quasi-static conditions can be observed in Berthellot tubes[7,8] mineral inclusions[9–11] trees[12–14] or fern sporangia[15–19] and lead to cavitation nucleation. Inspired by biological applications where cavitation is a drawback such as embolism[13–14] or a necessary triggering mechanism as for the fern catapult, microfabricated devices has been developed to study cavitation bubbles[20–23]. In these situations, the liquid is confined in micrometric compartments. The effects of the walls are of primary interest and constitute one of the motivations of the present study. Firstly the growth and dynamics of the bubble shall be strongly modified compare to the bulk case, but the walls will also strongly change the nucleation rate. Various theoretical and numerical studies have been devoted to understand and to predict nucleation rate. The comparison of continuous models (as the Classical Nucleation theory, CNT) to experiments leads to strong quantitative differences. In this theory, interfaces between phases are ideal, a balance between surface and volume forces generates an energy barrier to be passed by thermal fluctuations in order for a bubble to grow. Numerical simulations of the molecular dynamics of cavitation bubble nucleation in a stretched liquid have been carried out to calculate the nucleation rate, the barrier height and other thermodynamical parameters in different studies[24–36]. In that cases, the fluid is not confined and periodic conditions are used. We focus here on applying the CNT when walls are confining the liquid volume under tension, and performing Molecular Dynamics (MD) simulations al-

lows us to study the cavitation in a stretched Lennard-Jones liquid under confinement. This technique has also been used to study nanobubble behavior and stability.[37]

We present in a first part the classical CNT for homogeneous nucleation, then the effect of the confinement which modifies the free energy used in CNT, from.[22] We then point out the effect of walls (classical heteregeneous nucleation) and geometry through our modeling of planes, dihedrals and corners). In a second part we detail the simulation methods, how we detect bubbles and how we measure the expectation time τ. In a a third part, we show our results: 1) on our method to modify the contact angle: how does it vary with ϵ_{LS} ? 2) how τ does change with contact angle and depends on the nucleation location ?

Homogeneous nucleation and CNT

For a new phase to appear, an interface between liquid and vapor has to be created.[1] This new phase appears via the formation of localized nuclei in the bulk metastable phase. As a result of density fluctuations due to thermal noise, these small nuclei are formed and destroyed constantly in the metastable phase. In these conditions, we write the Free Energy function corresponding to the creation of a bubble of radius R in a stretched liquid as:

$$\Delta F_{homo}(R) = \frac{4\pi R^3}{3}\Delta p_0 + 4\pi R^2 \gamma \ , \tag{1}$$

where γ is the surface tension at the liquid/vapor interface, Δp_0 correspond to the depression of the metastable liquid $\Delta p_0 = (p - p_{sat}) < 0$ in the case of a homogeneous nucleation. In this expression p_{sat} is saturation pressure meaning the equilibrium pressure of coexistence of the two phases liquid and vapor, and p the negative metastable liquid pressure. When the critical bubble appears, it is in mechanical equilibrium, and we have:

$$\Delta p_0 = \frac{2\gamma}{R_c} \ . \tag{2}$$

In equation (2), R_c is the critical bubble radius. We write the reversible work needed for

the creation of a critical bubble as :

$$W^*_{homo} = \frac{16\pi\gamma^3}{3\Delta p_0^2} \ . \tag{3}$$

According to CNT, the mean expectation time τ_{homo} for a nucleation bubble is given by:

$$\tau_{homo} = A \exp(W^*_{homo}/k_b T) \ , \tag{4}$$

where A is a constant that we will calculate afterwards, and k_b is the Boltzmann constant. This time τ_{homo} depends on the liquid/vapor surface tension γ, the depression of the liquid Δp_0 and on temperature T.

The nucleation and growth of a bubble with confining walls will be modified on two aspects: i) The solid walls will induce heterogeneous nucleation events in addition to homogeneous ones. ii) The finite volume of the system will induce a constrained, finite growth of the bubble.

In the following, to compare heterogeneous and homogeneous events, we focus on the mean expectation time τ instead of the nucleation rate. This later is adapted for the bulk case, for a given volume V, and is given by: $J = 1/(\tau V)$. In our case with surfaces and corners, the use of the mean expectation time is more adapted.

Effect of the confinement

If we only take into account a free energy function like in equation (1), once the vapor bubble has reached the critical radius R_c, the bubble will grow infinitely as its energy will only decrease. In our work, we study the effect of a finite volume for the fluid domain, which is limited by impermeable walls. In that case, the size a bubble can reach will then be limited by the remaining liquid volume and the walls. Hence, the compressibility of the liquid and the wall rigidity will force the final bubble size, as it has been described by Vincent et al.[21] We write the isothermal compressibility κ_l of the liquid as:

$$1/\kappa_l = -V_l \left(\frac{\partial p}{\partial V_l} \right)_T \ . \tag{5}$$

In the case of small volume variations, *i.e* the bubble volume V_b is small compared to the liquid volume V_l, we assume that κ_l is approximately constant and writes:

$$\Delta p = -\frac{1}{\kappa_l} \frac{\Delta V_l}{V_l} \ . \tag{6}$$

For a spherical cavity with constant radius R_c (infinitely rigid and perfectly wetting walls), we write the free energy of the confined system, following Vincent et al.,[21] as:

$$\Delta F^c_{homo} = \frac{4\pi R^3 \Delta p_0}{3} \left(1 + \frac{1}{2\kappa_l \Delta p_0} \left(\frac{R}{R_c} \right)^3 \right) + 4\pi R^2 \gamma \ . \tag{7}$$

This new expression for the free energy brings out an equilibrium radius (Figure 1). Another effect of the confinement is to slightly increase the height of the nucleation barrier.

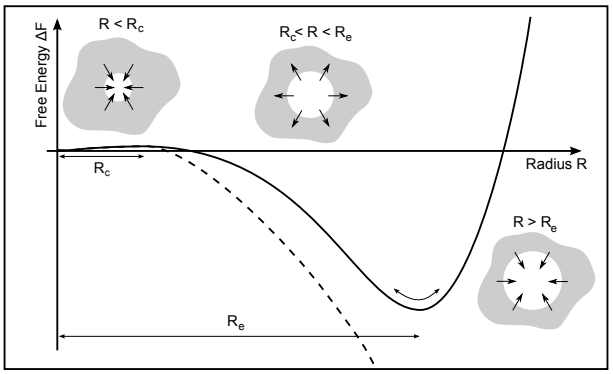

Figure 1: Schematic representation of the free energy of the system as a function of the radius R of the bubble: infinite liquid (dashed line), confined liquid (plain line).

Effect of the surface walls: Heterogeneous Nucleation on a flat surface

In most practical circumstances, suspended impurities or imperfectly wetted surfaces act as the interface on which the growth of a new phase is initiated. We consider the formation

of a nucleus at a solid/liquid interface, writing the free energy of the heterogeneous system, neglecting the confinement term in Eq. 7. We assume here that the equilibrium radius is large compare to the critical radius R_c in order for the change on the free energy due to the confinement effect to not affect the change on the nucleation barrier height. In addition, we consider only the case of one infinite wall :

$$\Delta F_{hete}(R) = \frac{\pi R^3}{3}(1+\cos\theta_m)^2(2-\cos\theta_m)\Delta p + \gamma S_{LV} + \gamma_{SV} S_{SV} - \gamma_{SL} S_{SV} \ , \tag{8}$$

with S_{LV} and S_{SV} respectively the surfaces of the Liquid/Vapor and Solid/Vapor interfaces, and γ, γ_{SV} and γ_{SL} respectively the surface tensions of the Liquid/Vapor, Solid/Vapor and Solid/Liquid interfaces. With the Young-Dupre Law,[43] we also have $\cos(\theta_m) = (\gamma_{SV} - \gamma_{SL})/\gamma$ and the free energy of the system becomes[1,38-39] :

$$\Delta F_{hete}(R) = \frac{\pi R^3}{3}(1+\cos\theta_m)^2(2-\cos\theta_m)\Delta p + \gamma(S_{LV} + S_{SV}\cos(\theta_m)) \ . \tag{9}$$

We have for a spherical cap: $S_{LV} = 2\pi R^2(1+\cos\theta_m)$, and also $S_{SV} = \pi R^2 \sin^2\theta_m = \pi R^2(1-\cos^2\theta_m)$. Then:

$$\Delta F_{hete}(R) = \pi R^2(1+\cos\theta_m)^2(2-\cos\theta_m) \times \left(\frac{R}{3}\Delta p + \gamma\right) \ . \tag{10}$$

Following again,[1] the work needed to nucleate a bubble on a solid plane is calculated by maximizing this free energy with R and taking the value at the maximum :

$$W^*_{hete} = \frac{16\pi\gamma^3}{3\Delta p^2}\frac{(1+\cos(\theta_m))^2(2-\cos(\theta_m))}{4} \ . \tag{11}$$

We observe that the work needed to create a new critical vapor bubble on a solid plane is the same as in the case of a homogeneous nucleation, multiplied by a geometric correction factor $W_{hete} = W_{homo}\psi(\theta_m)$ including the wetting angle θ_m between liquid and solid phases (Figure 7). This geometric factor $\psi(\theta_m)$ monotonically varies from 0 to 1 as the wetting angle θ_m decreases from 180 to 0 (Figure 2). This function is represented by the ratio of the truncated spherical bubble volume to the volume of a sphere with the same radius.

Effect of the surface walls: General case on multiple surfaces

In the case of a confining cavity in 3D, geometric effects must be added to the surface effect to fully describe the heterogeneous nucleation probabilities on multiple intersecting surfaces.

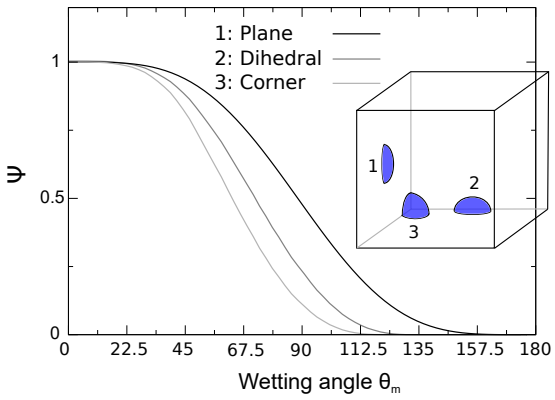

Figure 2: Variation of the three function ψ respectively from the right to the left, for a bubble on a plane, on two planes (dihedral) and on three planes (corner)

In fact, the function $\psi(\theta_m)$ is changing if the bubble nucleates at different locations of the liquid/solid interface. As this function represents the ratio of the truncated spherical bubble volume to the volume of a sphere that have the same radius, we numerically derive the variation of the three functions $\psi(\theta_m)$ for respectively a bubble nucleating on a plane, on a dihedral (intersection of 2 planes) and on a corner (intersection of 3 planes). These three

functions are represented on the Fig.2 which shows that for a vapor bubble it is energetically more favorable to nucleate on a corner (intersection of 3 planes), than a dihedral (intersection of 2 planes), than on a solid plane for a given wetting angle θ_m.

We now compare the mean expectation time in the case of homogeneous nucleation and heterogeneous nucleation: (By writing the following Eq.12, we neglect the trigonometric factor in the preexponential term[1]) :

$$\tau_{hete} = A \exp\left(\frac{W_{homo}}{kT}\psi(\theta_m)\right) \ . \tag{12}$$

This function gives a mean expectation time for a heterogeneous nucleation $\tau_h ete$. This time is equal to the time in the homogeneous case $\tau_h omo$ when the wetting angle θ_m is equal to 0, meaning a completely wetting surface. In the case of a homogeneous nucleation, we express the prefactor $A = \tau_{homo} \exp(-W_{homo}/kT)$, so we write the mean expectation time for the heterogeneous nucleation as :

$$\tau_{hete} = \tau_{homo} \exp\left(\frac{16\pi\gamma^3}{3kT}\left(\frac{\psi(\theta_m)}{\Delta p^2} - \frac{1}{\Delta p_0^2}\right)\right) \ . \tag{13}$$

With the Equation (13), we write the function ψ in terms of depression Δp and mean expectation time τ_{hete} :

$$\psi(\theta_m) = \frac{3\Delta p^2 k_b T}{16\pi\gamma^3} \log(\frac{\tau_{hete}}{\tau_{homo}}) + \frac{\Delta p^2}{\Delta p_0^2} \ . \tag{14}$$

Even if the presence of a solid surface always lowers the free energy barrier to create a bubble, a minimum value of the contact angle is required for the heterogeneous nucleation to become the predominant mechanism.[1] In practice, Equation (12) has a limited use because of the very irregular nature of surfaces on which heterogeneous nucleation takes place. In our MD simulations, as we control very precisely the geometrical surfaces between the liquid and solid atoms, we can study this effect. The process of heterogeneous nucleation is therefore limiting the extent of penetration into the metastable region, and is the reason why a negative

pressure is experimentally difficult to read.

EXPERIMENTAL: Simulation methods

Molecular dynamics parameters.

To study the nucleation of vapor bubbles, we use Molecular Dynamics simulations in the Canonical Ensemble using a Pre-compiled simulation code called LAMMPS.[40] This simulation method allows us to study the Classical Nucleation Theory, as this description takes into account an isothermal process for the appearance of the bubble. In this study, our system contains around 100000 interacting particles. The simulation box size for the liquid atoms was 40x40x40 σ.

We use the Shifted-Force truncated Lennard-Jones (LJ) pair potential :

$$\begin{aligned} u^{SF}(r \leq r_c) &= u^{LJ}(r) - u_c - (r - r_c)\left(\frac{dv}{dr}\right)_{r=r_c} \\ u^{SF}(r > r_c) &= 0 \ , \end{aligned} \tag{15}$$

with :

$$u^{LJ}(r) = 4\epsilon\left[\left(\frac{\sigma}{r}\right)^{12} - \left(\frac{\sigma}{r}\right)^{6}\right] \ , \tag{16}$$

where ϵ is the energetic depth of the potential, σ is the length at which the potential is equal to 0, and r is the distance between particles. The cut-off radius of the potential is taken equal to $r_c = 2.5\sigma$.

From now on we will use dimensionless units. The reduced units are the potential parameters σ and ϵ, and the particle mass m. We write the reduced distance $r^* = r/\sigma$, pressure $p^* = p\sigma^3/\epsilon$, density $\rho^* = \rho\sigma^3$, temperature $T^* = k_b T/\epsilon$, surface tension $\gamma^* = \gamma\sigma^2/\epsilon$, and time $t^* = t(\epsilon/m)^{1/2}/\sigma$. To integrate motion equations of the particle, we use the Verlet velocity algorithm. The time step is $0.05t^*$. The thermalisation of the system is carried out by the

Nose-Hoover Thermostat method.[41]

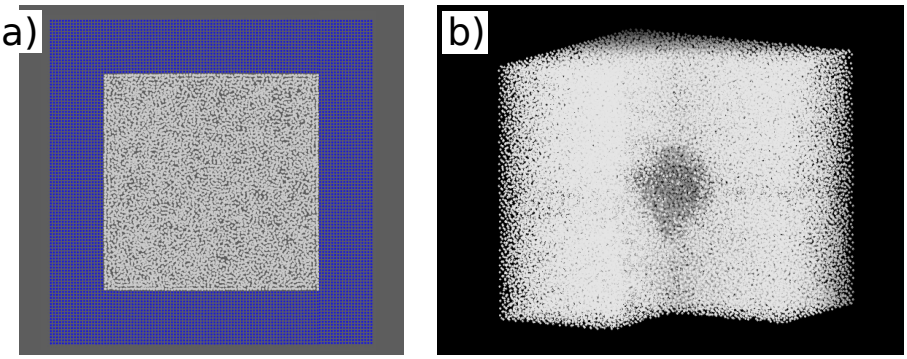

Figure 3: a) Picture of a slice of the 3D MD simulation. We see the "solid" atoms in blue, and the "liquid" atoms in white. b) Picture of only the "liquid" atoms with a corner from the center of the bubble removed, we see a cavitation bubble in the middle.

For the "solid" atoms we chose $\epsilon_{ss} = 100.0$ and for the "liquid" atoms we chose $\epsilon_{ll} = 1.0$, for both $\sigma = 1.0$. In this case, for a given temperature, a "solid" atom will need a higher energy to move than a "liquid" one. ϵ_{ls} will be varied.

The walls of the simulation box are simulated by 9-3 Lennard-Jones potential. This potential is obtained by integrating the potential energy between a L-J particle at the z position and a semi-infinite continuum below the plane $z = 0$, of uniformly distributed L-J particles.[42]

In order to have an energetically well equilibrated system, we first thermalise the "solid" atoms in the NVT ensemble for a characteristic time of 10^4 simulation steps. In a second time, we thermalise the "liquid" atoms at equilibrium density also in the NVT ensemble for 10^4 simulation steps. Then, we let the system "liquid + solid" (Figure 3) be equilibrated using a conjugate gradient algorithm, and thermalise for another 10^4 steps. This defines an initial thermalised configuration. We shall generate different starting (uncorrelated) states by performing a few extra 10^4 NVT simulation steps. Starting from one of these reference configuration, we devised the following algorithm in order to mimic an evaporation and reach a metastable state (that we call final state): (i) a random fraction (0.22%) of the liquid is removed (ii) the energy of the remaining liquid is minimized and (iii) a new thermalization with 10^4 simulation steps, during which we monitor that no cavitation takes place. Then

this is repeated for another fraction of the liquid atoms to go down to the expected pressure. Then we carry out at most 2 10^5 simulation steps of this stretched liquid, and go back to (i) if no bubble is detected meanwhile.

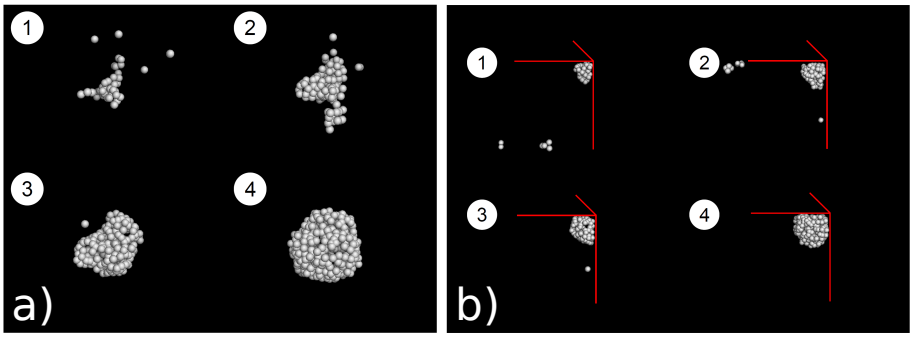

Figure 4: Temporal evolution of a cavitation bubble from the nucleation to its equilibrium radius for: a) a homogeneous nucleation and b) for an heterogeneous nucleation with the visualization of the corners of the cell.

Fig. 4 shows the evolution of a bubble from the nucleation to its final form. For the homogeneous case (Fig.4 a)), we see that at the beginning the bubble has a highly non-spherical shape. With time, more atoms come from the liquid bulk into the vapor bubble, and its shape become more and more spherical. For the heterogeneous case (Fig.4 b)), the bubble nucleates on a corner (upper-right) of the cell. The process is almost identical to the homogeneous case but the shape of the bubble follows the borders of the cell.

To limit the simulation time, the negative pressure used was varied as function of the contact angle. The highest one was used for the case $\theta_m = 0^o$: -0.25 and the lowest one was -0.6. Even in that case, we are not at the spinodal since from[30] its value is around -0.75 for $T^* = 0.8$.

Bubbles detection

To study and detect the nucleation of bubbles, we use a method based on Voronoi polyhedra analysis.[35] With this method, we quickly find out if a particle is in a liquid or vapor state (Figure 5). By defining a critical volume V_c when a particle is in vapor state and a critical number of particles N_c in vapor state to define a bubble, we directly detect the evolution

of the bubble volume as a function of time (Figure 6). In our simulations, we have chosen $V_c = 4.0\sigma^3$. With the distribution of the Voronoi volume of each atom in the liquid state, we observe that the probability of one atom in the liquid state to have a Voronoi volume higher than $4\sigma^3$ is almost 0 (for a stretched liquid in our configuration, it is estimated to 10^{-8}).

This method has also a great use in measuring the bubble size, as we directly obtain, by summing the volume of every particle, the bubble volume, and its variations with time.

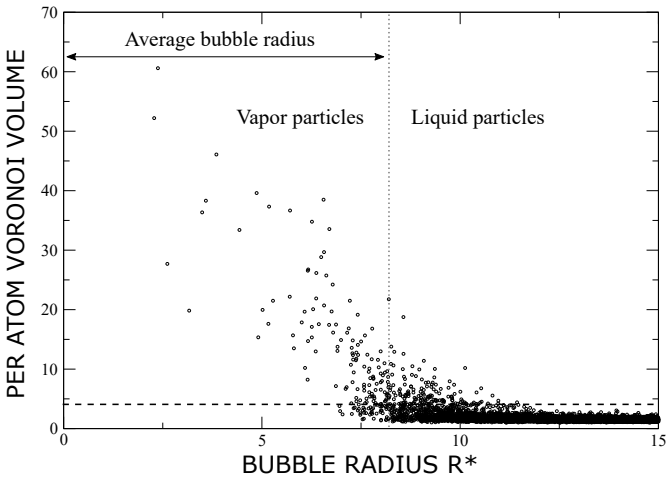

Figure 5: Radial distribution of the Voronoi volume of each atom centered at the center of the bubble. The horizontal line corresponds to the limit $V_c = 4\sigma^3$

The Figure 5 shows the radial distribution of the Voronoi Volume of each atom. When the system is at the liquid state (for the $R^* > 12$), every atom has a volume below $4.0\sigma^3$. When the bubble has its final size, we observe atoms inside the bubble having a Voronoi Volume going from $4.0\sigma^3$ (for atoms on the bubble surface) to $80.0\sigma^3$ (for atoms at the center of the bubble). We understand on this picture that this method is a straightforward way to guess in which state one atom is, and to compute the bubble size by a simple addition.

Mean expectation time

Figure 6 shows the bubble volume profiles for four events of cavitation in a LJ liquid. The time reading begins just after the system transfer to its final state. Every value of bubble volume on this plot has been averaged over 100 simulation steps. The cavitation time is

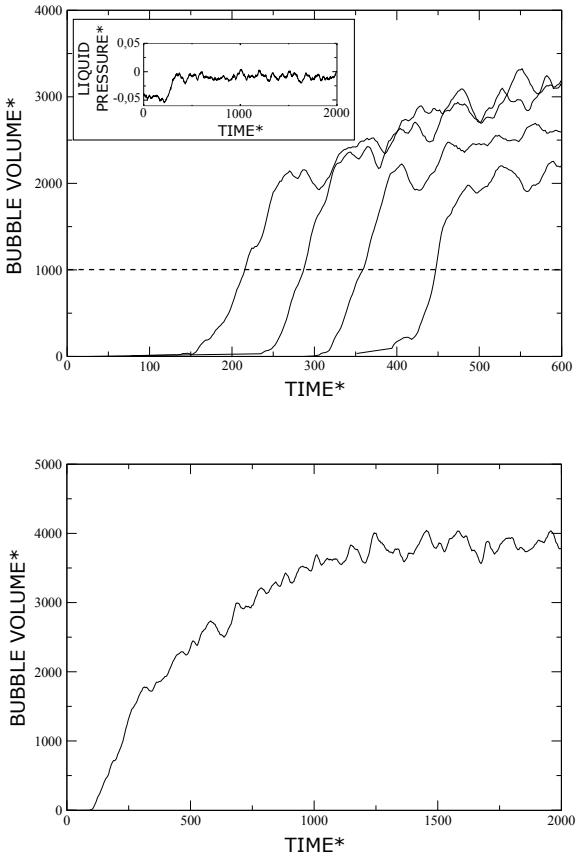

Figure 6: Top. Time dependence of the bubble volume for four molecular dynamics simulations of cavitation of a LJ liquid at $T^* = 0.8$ and $\rho^* = 0.6038$ in a system of $N = 60702$ atoms in the liquid state. In insert, is represented the liquid pressure as a function of time during the bubble nucleation. The liquid pressure reaches quickly equilibrium, but the volume reaches its equilibrium value in a longer time. Bottom: full length curve showing the evolution of the bubble volume. Due to reorganisation at the walls, the liquid volume decreases, consequently increasing the volume of the bubble.

defined when the bubble volume reaches 30% of the final bubble volume,as it corresponds to the fast growing period of the bubble. In the case presented on Figure 6, it corresponds to $R_b = 1000\sigma^3$, represented by the dashed line. A sufficiently large threshold ensure to avoid noise due to thermal movement and its value does not change the relative difference between the mean expectation time measured. We see on Figure 6 that the cavitation time τ is varying on different simulations. This variation arises from the probabilistic character of the nucleation. As the nucleation of a vapor bubble is considered as a rare event, the distribution of the cavitation time for different simulations with the same parameters follows a classical Poisson Law. We determine the mean expectation time of nucleation by taking average values over several simulations with the same conditions. It is valid when only one single critical nucleus is sufficient for the entire system to transform into the equilibrium fraction of liquid/vapor. This is the case in our MD simulations of a highly stretched liquid.

The second thing we learn from Figure 6, is that the volume of the bubble increases very quickly from almost 0 to a volume $V_{bubble} \approx 2000\sigma^3$. But we also notice that the bubble volume is still growing with a lower velocity. Meanwhile, we see the liquid pressure remaining, on average, constant over this longer timescale. The liquid pressure is represented in the insert in Figure 6. This slower volume growth is observed only in the case of liquid confined in a solid cell, and not for a fully periodic liquid. By sketching the spacial distribution of atoms in our simulations, we remark that once the liquid pressure comes back to a positive value, a few atoms tend to form a semi-organised layer next to, and due to the interaction with the solid part. The liquid pressure is represented on the insert in Figure 6 does not take into account these atoms. This observation leads to a decrease of the liquid atom number, so the bubble volume increase to deal with the equilibrium pressure to be constant. As this effect due to liquid and solid interaction is observed on longer timescales, it does not affect the bubble nucleation, but explains the shape of the curves on Figure 6.

RESULTS

Influence of the solid/liquid potential on the wetting angle in our system

The geometry of liquid particles placed in solid cell, allows us to control the liquid/solid wetting angle θ_m by varying only one parameter, namely the value of the potential parameter ϵ between the liquid particles and the solid ones. The influence of ϵ on the contact angle is defined on Figure 7. This set of measures were performed on a $N \approx 100000$ liquid particles, at the Temperature $T^* = 0.8$ as described in part . For a given interaction parameter ϵ, we measure the wetting angle on different cases, meaning different locations of the bubbles. The wetting angle is not dependent on the location.

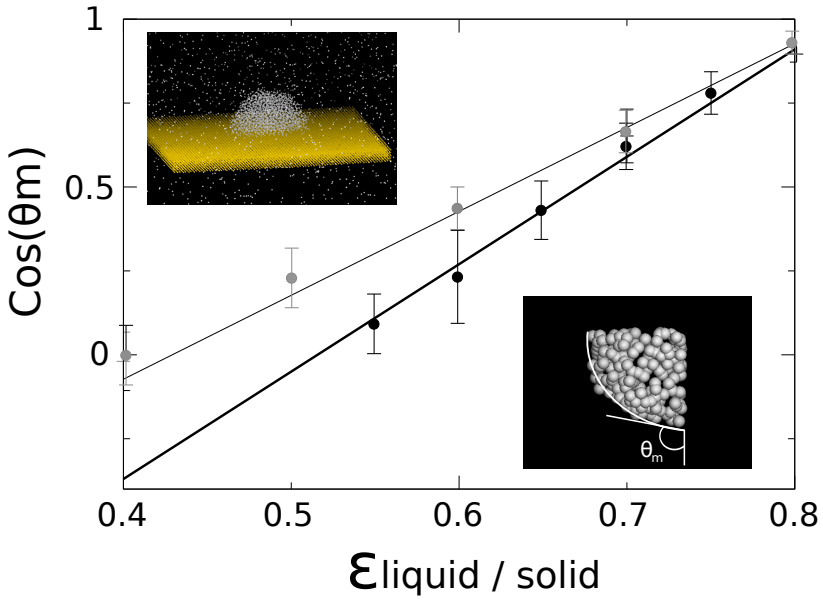

Figure 7: Dependence of the liquid/solid contact angle θ_m with the parameter ϵ between liquid and solid for a vapor bubble on a solid interface (bottom, black) and for a droplets on a solid surface (top, gray).

To acquire the value of the wetting angle, we approximate the surface of the droplet with a sphere as described on the Fig. 7. We find out that when we increase the potential

parameter ϵ between the liquid and solid particles, $\cos(\theta_m)$ increases linearly, meaning that the wetting angle θ_m decreases.

We performed other dedicated simulations to measure the contact angle for a droplets sitting on a solid surface. This is shown as the points in gray in Figure 7. We see that both curves are linear as function of ϵ_{ls}, the contact angles being larger in the bubble case compare to the droplet case.

For a Lennard-Jones potential, the surface tension between solid and liquid γ_{SL} is proportional to $-\epsilon/\sigma^2$. With this hint, it is clear that the variation of $\cos(\theta_m)$ linearly depends on the interaction between the liquid and solid particles.

Influence of the liquid/solid wetting on τ

Influence of the contact angle on τ

With our system, an interesting thing to study is the influence of the wetting angle θ_m on the mean expectation time for a cavitation bubble. As we saw in Eq.12, if we increase the wetting angle θ_m, it is easier for the system to nucleate a bubble. In fact, the measurement of a mean expectation time τ_{hete} by increasing the wetting angle for a given depression Δp becomes very difficult. To measure a τ_{hete} different than 0 (meaning that the bubble nucleates instantaneously), we also have to decrease the depression of the system. The Table 1 represents some interesting values to picture the effect of the wetting angle on the nucleation time τ_{hete}. The values are averages on sets of simulations. It clearly shows that for a given metastable state it is easier to nucleate a bubble by increasing the wetting angle, represented by a lower expectation time.

Table 1: Simulations values of mean expectation time τ for equivalent depression of the liquid before nucleation.

Interaction $\epsilon_{liquid/solid}$	Wetting angle θ_m	Expectation time τ
1.0	0	570
0.8	26	393
0.6	80	51

Determination of the function $\Psi(\theta_m)$

As we see on Eq.14, we have normalized our measurement by the depression Δp of the system with the depression Δp_0 in the homogeneous case. In our computation, we have to evaluate τ_{homo}, Δp_0, τ_{hete} and Δp. By putting these values in Eq.14, we shall obtain the value of the function Ψ. Here we use the value of the surface tension $\gamma = 0.396$ as an average surface tension given on multiple references, represented in Table 2. The values to calculate Ψ are summarized in table 3.

Table 2: Values of the surface tension given in litterature

T^*	Method	Surface tension γ	Reference
0.80	MC	0.405 ± 0.003	Trokhymchuk et al.[28]
0.80	MD	0.408 ± 0.018	Trokhymchuk et al.[28]
0.80	MD	0.39 ± 0.01	Nijmeijer et al.[24]
0.80	MD	0.388 ± 0.004	Haye and Bruin[27]
0.80	MD	0.39 ± 0.02	Adams and Henderson[26]

Normalization from the spatial position of nucleation: effect of the geometry

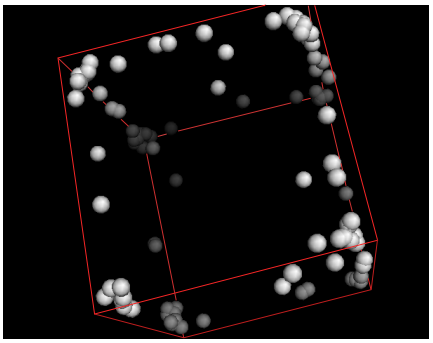

Figure 8: Location of a hundred of nucleations inside a solid cell. We clearly see that in a majority of case, the location of the nucleation is a corner (intersection of 3 plans)

If we plot directly the values of Ψ on Figure 2, we see that they are between these three curves. The explanation of this, is that the location of the bubble nucleation cannot be defined with these parameters. For a given Δp and θ_m the bubble has a certain probability

to nucleate on a plane, on a dihedral and on a corner. In different conditions, we can measure the proportion of bubbles nucleating in different parts of the cell. Our measurements clearly shows that the proportion of bubbles nucleating on different parts of the cell is independent of the wetting angle. for example, for two contact angles (80ř and 25 ř), the proportions in different locations are respectively for corners: 68.9 % / 69.5 %, dihedral: 25.7 % / 26.1 %, planes: 5.4 % / 4.4 %. Bulk: 0.0 % / 0.0 %.

On average, the proportion of bubbles nucleating on a corner, is the largest, is 69.2%, the proportion of bubbles nucleating on a dihedral is 25.9%, the proportion of bubbles nucleating on a plane is 4.9%. Figure 8 shows a representation of the nucleation sites for a set of a hundred simulations. We clearly see that a majority of bubbles nucleates on the corner of the solid cell.

As we now know, the probability for a bubble to appear in the three different locations of the solid cell, we estimate the mean value of the function Ψ, normalized by the mean location of the nucleation of the bubble Ψ'. This function is given by $\Psi' = 0.692\Psi_{3p} + 0.259\Psi_{2p} + 0.049\Psi_{1p}$.

Table 3: Simulations values to calculate $\Psi(\theta_m)$.

τ_{homo}	Δp_0	Ψ
131.7447	0.5808	1.0000
τ_{hete}	Δp	Ψ
123.2211	0.6004	1.0459 ± 0.0736
327.2889	0.5103	0.9953 ± 0.0279
465.8154	0.4694	0.9159 ± 0.0561
613.7895	0.4155	0.7621 ± 0.0542
699.0540	0.3561	0.5754 ± 0.0601
602.7879	0.2936	0.3791 ± 0.0877
477.5800	0.2547	0.2711 ± 0.0464

Fig.9 shows the evolution of the function Ψ' controlling the effect of the wetting angle on the mean expectation time of a nucleation. The values of the dots are calculated from the measured values of τ_{hete} using Eq.13. We clearly get a very good agreement between the measured values and the theoretical values of the function Ψ' without any free parameter in

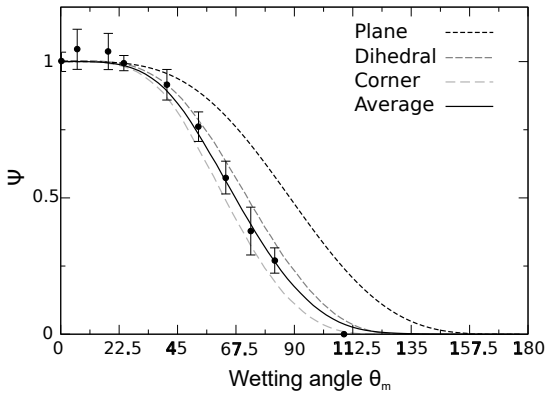

Figure 9: Evolution of the function Ψ' as a function of the wetting angle θ_m. The disks are the simulated measurements and the lines are the theoretical function. The full line corresponds to the function Ψ'.

the model.

After nucleation, the bubbles presents an oscillating regime before reaching their equilibrium radius due to the confinement, this is observed on the Figure 6. It shows oscillations of the bubble volume and as a consequence, in the liquid pressure. This observation has been studied experimentally by O. Vincent.[21] We will present later our results on these oscillations and their possible consequences for the multi cavities case.

CONCLUSION

In this paper, our goal is to understand the effect of a solid confinement on the nucleation of vapor bubble in a highly stretched liquid. We use MD simulations to compute this system in the Canonical ensemble. All these simulations were carried out with a fixed temperature $T^* = 0.8$. By changing the interaction between the liquid atoms and the solid atoms, we control the wetting angle very precisely.

We first study the influence of the interaction parameter ϵ on a vapor bubble on planes in different geometries. The measurement of the wetting angle θ_m is performed by approximating the surface of the vapor bubble with a portion of sphere and its angle with the

solid plane. We have shown that $\cos(\theta_m)$ increases linearly with the potential parameter ϵ between the liquid and the solid phases. We compare these angles to other simulations done on simple droplets on plane system. Both values evolve linearly with ϵ_{ls}, but with a slightly different coefficient.

Then the main goal of this work is to understand the effect of the wetting angle on the nucleation of vapor bubbles. The MD simulations are very convenient for this study to make this statistical measurements, as the nucleation is a probabilistic phenomenon. We use a method based on the Voronoi volumes to detect the nucleation of the bubble and to have very easily access to its size, position and shape. By measuring the cavitation mean expectation time for different wetting angles, we could compare to the CNT adapted to the heteregeneous case on planes, dihedrals and corners. We found a very good agreement for the ratio between heterogeneous and homogeneous mean expectation times with the CNT, providing that the in-situ contact angles measured are used. We can then predict very precisely, even though the probabilistic character of the nucleation, how the wetting angle influence the appearance of a bubble, knowing that small-scale or geometrical effects are quantitatively expressed in the value of an effective contact angle, different from the one obtained for droplets on a plane.

References

(1) Debenedetti, P.G., Metastable Liquids: Concepts and Principles, *Princeton University Press* (1996)

(2) Dhir, V.K. Boiling heat transfer. Annual Review of Fluid Mechanics, Vol. **30**, p.365-401 (1998)

(3) Martynyuk, M.M., Phase explosion of a metastable fluid, Combustion, Explosion and Shock Waves, **13**, Issue 2, pp 178-191 (1977)

(4) Brujan, E.A. Cavitation in non newtonian fluids. *Springer* (2011)

(5) Suslick, K. S. Sonochemistry. Science. **247**, 1439-45 (1990).

(6) Brennen, C. E. Cavitation and Bubble Dynamics. *Oxford University Press* (1995)

(7) Berthelot, M. Ann. Chim. Phys. 1850, **30**, 232-237.

(8) Briggs, L. J. Limiting negative pressure of water. J. Appl. Phys. **21**. pp. 721-722 (1950)

(9) Zheng, Q., Durben, D. J., Wolf, G. H. and Angell, C. A. Science **254**, 829-832 (1991).

(10) Caupin, F., Herbert, E. C. R. Physique, **7**, 9-10, pp. 1000-1017 (2006). Cavitation in water: a review.

(11) Azouzi, M.E.M., Ramboz, C., Lenain; J.F. and Caupin, F. A coherent picture for water at extreme negative pressure. Nature Physics. **9**, 38 (2013).

(12) Tyree M.T., Zimmermann M.H., Xylem Structure and the Ascent of Sap, *Springer*, 2nd ed. (2003)

(13) Tyree M. T., Davis S. D. and Cochard H. Biophysical Perspectives of Xylem Evolution: is there a Tradeoff of Hydraulic Efficiency for Vulnerability to Dysfunction? IAWA Journal, Volume **15**, Issue 4, p. 335-360 (1994)

(14) N. M. Holbrook, M. J. Burns, and C. B. Field. Negative xylem pressures in plants : a test of the balancing pressure technique. Science, **270**, No. 5239, pp. 1193?1194 (1995)

(15) Renner O., Jahr Wiss Bot., **56**, p. 647 (1915)

(16) Ursprung A., ber Deut Bot. Ges., **33**, p. 153 (1915)

(17) Ritman, K.T. and Milburn, J. A. Journal of Experimental Botany. **41**, No. 230, pp. 1157-1160 (1990)

(18) X. Noblin, NO Rojas, J Westbrook, C. Llorens, M Argentina and J Dumais. The fern sporangium: a unique catapult. Science, **335**, 6074, pp. 1322-1322 (2012).

(19) Llorens, C., Argentina, M., Rojas, N., Westbrook, J., Dumais, J., Noblin, X. The fern cavitation catapult: mechanism and design principles. Journal of the Royal Society Interface, **13**, 114 (2016)

(20) Wheeler, T. D., Stroock, A. D. The transpiration of water at negative pressures in a synthetic tree. Nature, **455**, P. 208-212 (2008).

(21) Vincent, O., Marmottant, P., Quinto-Su, P.A. and Ohl, C.D. Birth and Growth of Cavitation Bubbles within Water under Tension Confined in a Simple Synthetic Tree. Phys. Rev. Lett. **108**, 184502 (2012).

(22) Vincent, O., Marmottant, P., Gonzalez-Avila S.R., Ando, K., and Ohl, C.D. The fast dynamics of cavitation bubbles within water confined in elastic solids. Soft Matter **10** (10), 1455-1461 (2014)

(23) Scognamiglio, C., Magaletti, F., Izmaylov, Y., Gallo, M., Casciola, C.M., Noblin, X. The detailed acoustic signature of a micro-confined cavitation bubble. Soft matter **14** (39), 7987-7995 (2018)

(24) M. J. P. Nijmeijer, A. F. Bakker, and C. Bruin. A molecular dynamics simulation of the Lennard-Jones liquid-vapor interface. J. Chem. Phys. **89**, 3789 (1988)

(25) Zeng X. C. and Oxtoby, D. W. Gas-liquid nucleation in lennard-jones fluids. J. Chem. Phys. **94**, no. 6, 4472-4478, 1991.

(26) Adams, P., and Henderson, J. R., Molecular dynamics simulations of wetting and drying in LJ models of solid-fluid interfaces in the presence of liquid-vapour coexistence. Mol. Phys., **73**, 1383 (1991)

(27) Haye, M. J., and Bruin, C. Molecular dynamics study of the curvature correction to the surface tension. J. Chem. Phys, **100**, 556 (1994)

(28) Trokhymchuk, A. and Alejandre, J. Computer simulations of liquid/vapor interface in Lennard-Jones fluids: Some questions and answers. J. Chem. Phys, **111**, 8510 (1999)

(29) Shen, K. and P. G. Debenedetti, P.G. A Computational Study of Homogeneous Liquid-Vapor Nucleation in the Lennard-Jones Fluid. J. Chem. Phys. **111**, 3581 (1999).

(30) V. K. Shen and P. G. Debenedetti, J. Chem. Phys. **114**, 4149 (2001).

(31) Amanda J. Page and Richard P. Sear. Heterogeneous Nucleation in and out of Pores. Phys. Rev. Lett. 97, 065701 (2006)

(32) Wang, J., Valeriani, C. and Frenkel, D. J. Homogeneous bubble nucleation driven by local hot spots: A molecular dynamics study. The Journal of Physical Chemistry B, **113**, no. 12, 3776-3784, 2009.

(33) Stacey L. Meadley and Fernando A. Escobedo. Thermodynamics and kinetics of bubble nucleation: Simulation methodology. J. Chem. Phys. 137, 074109 (2012).

(34) Alberto Giacomello, Mauro Chinappi, Simone Meloni and Carlo Massimo Casciola. Geometry as a Catalyst: How Vapor Cavities Nucleate from Defects. Langmuir 29, 14873?14884 (2013).

(35) Jose LF Abascal, Miguel A Gonzalez, Juan L Aragones and C Valeriani. Homogeneous bubble nucleation in water at negative pressure : A Voronoi polyhedra analysis. J. Chem. Phys, **138**, 084508 (2013)

(36) V. G. Baidakov and K. S. Bobrov. Spontaneous cavitation in a lennard-jones liquid at negative pressures. J. Chem. Phys, **140**, no. 18 (2014).

(37) S. Maheshwari, M. van der Hoef, X. Zhang, and D. Lohse. Stability of surface nanobubbles: A molecular dynamics study. Langmuir **32**, 11116 (2016)

(38) Simone Meloni, Alberto Giacomello and Carlo Massimo Casciola. Focus Article: Theoretical aspects of vapor/gas nucleation at structured surfaces. J. Chem. Phys. 145, 211802 (2016).

(39) V. P. Skripov, Metastable Liquids (Halsted Press, 1972).

(40) S. Plimpton, Fast Parallel Algorithms for Short-Range Molecular Dynamics. J. Comp. Phys, **117**, 1-19 (1995)

(41) D. J. Evans and B. L. Holian, The Nose-Hoover thermostat. J. Chem. Phys, **83**, 4069 (1985)

(42) J.N. Israelachvili. Intermolecular and surface forces, *Academic Press*, 3rd ed. (2011).

(43) T. Young. An Essay on the Cohesion of Fluids. Philos. Trans. R. Soc. London **95**, 65 (1805)

Acknowledgement

This study was supported by the "Agence Nationale de la Recherche" (Young researcher project, CAVISOFT : ANR-10-JCJC-0407), by the CNRS (Centre Nationale de la Recherche Scientifique, INP institute) and the Region PACA (Region Provence Alpes Cote d'Azur). This work was granted access to the HPC and visualization resources of ?Centre de Calcul Interactif? hosted by ?Université Côte d?Azur?.

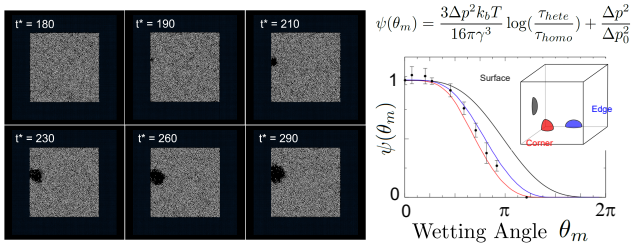

Graphical TOC Entry